Transp Porous Med (2010) 82:247–274
DOI 10.1007/s11242-009-9474-2

Numerical Simulations of the Thermal Impact of Supercritical CO_2 Injection on Chemical Reactivity in a Carbonate Saline Reservoir

Laurent André · Mohamed Azaroual · André Menjoz

Received: 17 December 2008 / Accepted: 11 September 2009 / Published online: 29 September 2009

Abstract Geological sequestration of CO_2 offers a promising solution for reducing net emissions of greenhouse gases into the atmosphere. This emerging technology must make it possible to inject CO_2 into deep saline aquifers or oil- and gas-depleted reservoirs in the supercritical state ($P > 7.4$ MPa and $T > 31.1$°C) to achieve a higher density and therefore occupy less volume underground. Previous experimental and numerical simulations have demonstrated that massive CO_2 injection in saline reservoirs causes a major disequilibrium of the physical and geochemical characteristics of the host aquifer. The near-well injection zone seems to constitute an underground hydrogeological system particularly impacted by supercritical CO_2 injection and the most sensitive area, where chemical phenomena (e.g. mineral dissolution/precipitation) can have a major impact on the porosity and permeability. Furthermore, these phenomena are highly sensitive to temperature. This study, based on numerical multi-phase simulations, investigates thermal effects during CO_2 injection into a deep carbonate formation. Different thermal processes and their influence on the chemical and mineral reactivity of the saline reservoir are discussed. This study underlines both the minor effects of intrinsic thermal and thermodynamic processes on mineral reactivity in carbonate aquifers, and the influence of anthropic thermal processes (e.g. injection temperature) on the carbonates' behaviour.

Keywords Coupled modelling · Supercritical CO_2 · Saline reservoir · Joule–Thomson effect · Geochemical reactivity

1 Introduction

Carbon dioxide (CO_2) storage in saline reservoirs is a promising alternative for the sequestration of this greenhouse gas due to their capacity worldwide (Bachu 2002; IPCC 2005).

L. André (✉) · M. Azaroual · A. Menjoz
BRGM – Water Division, 3 Avenue Claude Guillemin, BP 36009, 45060 Orleans Cedex 2, France
e-mail: l.andre@brgm.fr
URL: www.brgm.fr

Results of modelling studies suggest that under favourable conditions CO_2 can be safety confined for thousands of years (Weir et al. 1996a,b; White et al. 2005). However, before effective and safety containment can be ensured in a selected aquifer, investigations need to be carried out on reservoir behaviour when subjected to physical, chemical and thermal perturbations induced by massive CO_2 injection. If laboratory or field experiments can bring many details about gas behaviour in targeted reservoirs, numerical simulations constitute an integrative tool of main importance to assess specific processes and various feedbacks able to occur during CO_2 injection and storage.

In a previous article (André et al. 2007), the reactivity of supercritical CO_2 injection was analysed and compared to the reactivity of acidified water. While reservoir properties do not seem to be drastically affected by the injection of supercritical CO_2, simulated scenarios highlighted the high chemical reactivity of the near-well region. Both compensating and amplifying processes were identified, depending on the duration of the injection period and the location of the injection well within the reservoir. First, injected supercritical CO_2 dissolves in the aqueous solution, thus increasing both water acidity and mineral dissolution potential, favouring an increase in porosity, which may be beneficial to CO_2 injectivity. However, numerical simulations of massive injection show that hydraulic processes constrained by supercritical CO_2 injection then desiccate the near-well porous medium. After gas dissolution, the continuous injection of CO_2 displaces the water in the porous medium: mobile water is removed by the injected dehydrated supercritical CO_2 (Mahadevan 2005; Mahadevan et al. 2007). The duration of this displacement period depends on the relative permeability and capillary pressure of the porous medium. At the end of this step, immobile residual water, trapped in pores or distributed on grain surfaces as a thin film, is in contact with the continuous dry CO_2 flux (i.e. without water vapour). Consequently, continuous and extensive evaporation leads to both the appearance of a drying front moving into the medium and the precipitation of salts and possibly secondary minerals. All of these processes can have an impact on the porosity and permeability of the medium. Moreover, they can influence long-term well injectivity.

The principal aim of this study was to include all the thermal, hydraulic and chemical (THC) processes in fully coupled simulations. The study focused on a specific fictive case in which supercritical CO_2 is injected into a carbonate reservoir with properties similar to those of the Dogger aquifer in the Paris Basin (mid-Jurassic). This saline carbonate reservoir is the object of several studies co-funded by the French National Agency for Research (ANR) for the development of a future geological CO_2 storage pilot-project (e.g. André et al. 2007; Vidal-Gilbert et al. 2009 and references cited therein). The study reported here goes further than our previous investigations (André et al. 2007) and analyses the chemical reactivity when influenced by numerous parameters including thermal properties. In the framework of CO_2 storage, the impact of temperature on water/rock exchanges (mass and heat, for instance) around the wellbore was evoked by Marcolini et al. (2008). But, this kind of coupled approach is not much documented and few authors have, as yet, described in details the impact of CO_2 injection temperature on reactivity and mass exchanges between phases in such targeted reservoir systems (residual brine-host rock-supercritical CO_2).

After reviewing the different thermal processes that can occur at the reservoir scale (heat of CO_2 dissolution, water evaporation, Joule–Thomson effect, injection temperature and heat transfers to and from confining beds), we analyse two injection scenarios:

– Injection of supercritical CO_2 at a low flow rate ($1\,kg\,s^{-1}$ equivalent to 0.03 Mt per year) in a 2D radial model in non-isothermal mode at the reservoir temperature (75°C) and at

a lower temperature (40°C). The behaviour of the near-well region is studied by integrating the vertical component (gravity effect).
– Injection of supercritical CO_2 at a high flow rate ($20\,kg\,s^{-1}$ equivalent to 0.6 Mt per year) and low temperature (40°C) to determine the impact of a low CO_2 temperature on the chemical reactivity of the system and the mass exchanges between phases. This simulation allows us to study the chemical reactivity of the system in response to a massive cooling of the reservoir.

Within the framework of numerical simulations of coupled processes (THC), these two scenarios should enable us to determine the spatial chemical reactivity of the reservoir system as a function of pressure and temperature gradients and gas saturation.

2 Thermal Processes During CO_2 Injection

The properties of pure CO_2 are highly dependent on temperature and pressure conditions. Moreover, depending on T and P conditions, CO_2 can exist in different states (gas, liquid or supercritical for temperatures and pressures higher than 31.4°C and 7.35 MPa, respectively). The thermodynamic state of CO_2 will determine physical properties such as density, viscosity and enthalpy. In the case of CO_2 storage in deep geological reservoirs, numerical simulations should be done in non-isothermal mode to take into account the thermal processes. The preliminary geochemical impact estimated for the CO_2-enhanced geothermal systems (Brown 2000; Pruess 2008) showed the potential expansion of the heat exchange surfaces and the targeted reservoir volumes (Pruess and Azaroual 2006). Oldenburg (2007) highlights the heat exchanges between fluids and rock in relation with the heat capacity of the rock formation for CO_2 injection into depleted gas reservoirs. All of these thermal behaviours confirm the need of taking temperature into account for CO_2 storage in deep saline aquifers.

The thermal processes that might occur in the reservoir have different origins and non-intuitive combined impacts. Some of them are associated with petrophysical properties (such as the heat transfer between the host reservoir and confining beds), while others can have a thermodynamic origin (e.g. the heat of CO_2 dissolution, the water evaporation, the Joule–Thomson effect) or an anthropic origin (e.g. the CO_2 injection temperature, which is determined at the wellhead).

The principal temperature processes that might occur in the reservoir during CO_2 injection and storage are described below.

2.1 Heat Transfers Between the Host Reservoir and Confining Beds

The temperature within deep reservoirs depends on the local geothermal gradient. Before any CO_2 is sequestered, a temperature continuum exists between the caprock, the reservoir and the basement. During reservoir exploitation, the temperature can be modified due, for instance, to the injection of fluids that are colder or hotter than the formation fluid. If temperature variations are expected within the reservoir, the impervious confining beds tend to buffer these variations. Heat transfer between the confining beds and the reservoir fluids can impact the reservoir temperature, in particular, near the reservoir/basement and reservoir/caprock interfaces. Consequently, we expect to find chemical reactivity in the middle of the reservoir different from that along the upper and lower boundaries with the confining beds. The impact of these heat transfers will depend, however, on reservoir thickness: heat exchanges will have a greater impact in a thin reservoir than in a thick one, which has a higher thermal inertia.

2.2 Heat of CO_2 Dissolution

The dissolution of gases in aqueous saline solutions under high pressure and temperature is of major importance for geological storage. Studies of CO_2 dissolution in water at different temperatures, pressures and water salinities have been reported by many authors due to their influence on the density, viscosity and specific enthalpy of brine (e.g. Spycher and Pruess 2005; Koschel et al. 2006). Literature data show that the heat-of-dissolution of CO_2 in water is exothermic at the typical reservoir temperature and decreases in absolute value with both increasing temperature and pressure. In the case of CO_2 storage in deep saline aquifers, CO_2 dissolution in brine will produce a slight local increase in temperature.

2.3 Latent Heat of Water Vapourization

As energy is needed to overcome the molecular forces of attraction between liquid water particles (H_2O molecules and bearing electrolytes), the transition of liquid water to vapour requires the input of energy causing a drop in temperature in the surrounding medium. If the water vapour condenses back to a liquid or solid phase onto a surface, the latent energy absorbed during evaporation is released as sensible heat. The latent heat of water vapourization is 2,260 kJ kg^{-1} at 100°C and 0.1 MPa. The drying-out caused by CO_2-induced vapourization implies cooling due to these latent heat effects.

2.4 The Joule–Thomson Effect

The Joule–Thomson effect is a thermodynamic process (also called a throttling process) related to isenthalpic expansion of real gases. Possible Joule–Thomson cooling corresponds to a drop in temperature when a real gas expands from high to low pressure at constant enthalpy. The coefficient arising in a Joule–Thomson process, μ_{JT}, is defined by:

$$\mu_{JT} = \left(\frac{\partial T}{\partial P}\right)_H \approx \frac{\Delta T}{\Delta P}, \tag{1}$$

where T is the temperature, P is the pressure and H is a partial derivative at constant enthalpy. Figure 1 shows that Joule–Thomson coefficients are greater at low pressure than at pressures higher than 7 MPa, i.e. about 0.5 K MPa^{-1} at 40°C and 20 MPa and about 20 times higher at the same temperature and 5 MPa.

Therefore, the Joule–Thomson effect will be greatest in cases of CO_2 storage in depleted gas fields with low pressure (e.g. Oldenburg 2007). For CO_2 storage in saline aquifers at depths greater than 700 m (pressure higher than 7 MPa), a weak Joule–Thomson effect is expected (Bielinski et al. 2008). Nevertheless, even if this thermal effect is limited in deep aquifers and hydrodynamic and transport properties are weakly influenced by cooling, the amplitude of the Joule–Thomson coefficient is non-negligible and may combine with other thermal processes (described above) to induce a significant cumulative effect.

2.5 Injection Temperature

Downhole injection temperature will control many fundamental processes (e.g. thermo-chemical, thermo-mechanical). This injection temperature is dependent on the PVTX properties (pressure, volume, temperature and composition) of the injected gas stream. It also depends on wellhead conditions (which are subject to operational, economic, legal, engineering and safety constraints), well completion and many other parameters, such as

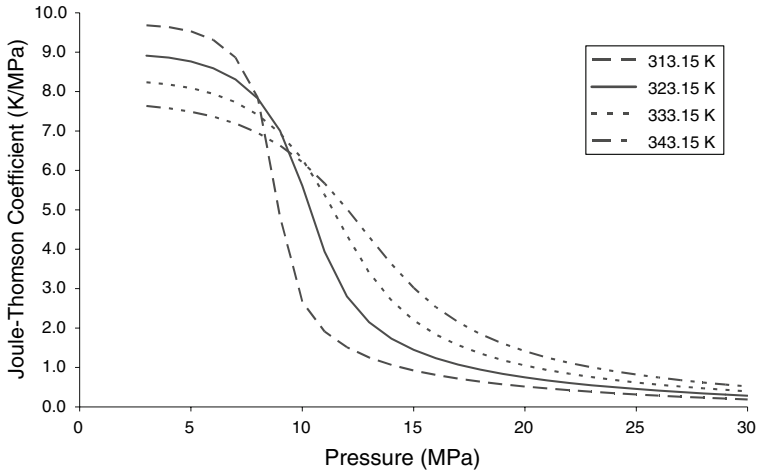

Fig. 1 Joule–Thomson coefficient for CO_2 as a function of pressure and temperature (data from NIST Webbook)

pressure losses and heat exchange along the wellbore. Phase changes can be expected in the well for specific cases due to these complex thermodynamic processes. The determination of downhole temperature has not yet received much attention and few bibliographic data exist. Bielinski et al. (2008) suggested a downhole CO_2 temperature ranging from 40 to 60°C for an injection well targeting a host reservoir about 700 m deep with an initial temperature between 33 and 36°C. Some recent articles present also attempts to model CO_2 flow in the injection wellbore (Pruess 2004; Lu and Connell 2008; Pan et al. 2008; Paterson et al. 2008).

3 Numerical Tool and Modelling Approach

3.1 Numerical Tool

The TOUGHREACT simulator (Xu and Pruess 2001) was used for all the simulations in this study. This code couples thermal, hydrologic and chemical (THC) processes and is applicable to one-, two-, or three-dimensional geologic systems with physical and chemical heterogeneity. ECO2n (Pruess 2005), a fluid property module for TOUGH2 V2 (Pruess et al. 1999) was developed specifically to model isothermal or non-isothermal multiphase flow in water/brine/CO_2 systems. Actually, apart the heat transfer through confining beds, all the other processes presented in Sect. 2 derives from the description of thermodynamics which is accomplished by ECO2n for H_2O–CO_2–NaCl mixtures.

TOUGHREACT simulates the chemical reactivity of the system based on a thermodynamic database, which is an extension of the EQ3/6 database (Wolery 1992) for the 0–300°C range, 1 bar below 100°C and water saturation pressure above 100°C.

The current TOUGHREACT version uses an extended Debye–Hückel model (Helgeson et al. 1981) to determine activity coefficients of dissolved species:

$$\begin{aligned} \mathrm{Log}\,(\gamma_i) = &-\frac{A_\gamma z_i^2 I^2}{1 + \text{å}\, B_\gamma I^{1/2}} + \mathrm{Log}(1 + 0.0180153 m^*) \\ &- \left[\omega_i b_{\mathrm{NaCl}} + b_{\mathrm{Na^+,Cl^-}} - 0.19\,(|z_i| - 1)\right] I, \end{aligned} \tag{2}$$

where i refers to each ion, γ is the activity coefficient of the ion, z is the ion electric charge, m^* is the total molality of all species in solution, I is taken as the true ionic strength of the solution, ω is the Born coefficient, b_{Na^+,Cl^-}, b_{NaCl}, are Debye–Hückel parameters and å is calculated from ion radii.

A_γ and B_γ, temperature and pressure dependent parameters, were calculated according to Lassin et al. (2005). The new values for A_γ and B_γ are $0.5568\,kg^{1/2}\,mol^{-1/2}$ and $0.3367 \times 10^{10}\,kg^{1/2}\,mol^{-1/2}\,m^{-1}$ at 200 bars and 75°C, respectively, when compared to $0.5095\,kg^{1/2}mol^{-1/2}$ and $0.3284 \times 10^{10}\,kg^{1/2}\,mol^{-1/2}\,m^{-1}$ at 1 bar pressure and 25°C.

André et al. (2007) did calculations with TOUGHREACT and an in-house code, SCALE2000 (Azaroual et al. 2004), a geochemical simulator designed for highly saline solutions. There are discrepancies between the two codes and conclusions highlight the advantage of using the Pitzer formalism rather the Debye–Hückel for ionic strength higher than 0.5–0.7. Nevertheless, TOUGHREACT enables a first qualitative approach to the main geochemical processes and general evolutionary trends of the system.

Mineral dissolution and precipitation reactions occur under kinetic conditions. The general form of the rate law proposed by Lasaga (1984) and Steefel and Lasaga (1994) is applied for mineral dissolution and precipitation:

$$r_n = \pm k_n A_n \left|1 - \Omega_n^\theta\right|^\eta \tag{3}$$

A positive value for r_n ($mol\,s^{-1}$) corresponds to dissolution of the mineral n (negative for precipitation), k_n is the rate constant ($mol\,m^{-2}\,s^{-1}$) depending on the temperature, A_n is the specific reactive surface area ($m^2\,kg_w{}^{-1}$) and Ω_n is the saturation ratio of the mineral n ($\Omega_n = Q/K$). The empirical parameters θ and η are determined from experiments, otherwise they are usually taken as 1.

The dependence of the rate constant k with temperature is calculated by means of the Arrhenius equation:

$$k = k_{25} \exp\left[\frac{-E_a}{R}\left(\frac{1}{T} - \frac{1}{298.15}\right)\right], \tag{4}$$

where E_a ($J\,mol^{-1}$) is the activation energy, k_{25} ($mol\,m^{-2}\,s^{-1}$) the rate constant at 25°C, R ($J\,K^{-1}\,mol^{-1}$) is the universal gas constant and T (K) the absolute temperature.

The dissolution and precipitation of alumino-silicates and salts can be controlled by the H^+ concentration (acid mechanism) and the OH^- concentration (alkaline mechanism) in addition to the neutral mechanism corresponding to Eq. 4. In this case, r_n is calculated using the following extended equation:

$$r_n = \left[\begin{array}{l} k_{25}^{nu} \exp\left[\frac{-E_a^{nu}}{R}\left(\frac{1}{T} - \frac{1}{298.15}\right)\right] \\ \quad + k_{25}^{H} \exp\left[\frac{-E_a^{H}}{R}\left(\frac{1}{T} - \frac{1}{298.15}\right)\right] a_H^{n_H} \\ \quad + k_{25}^{OH} \exp\left[\frac{-E_a^{OH}}{R}\left(\frac{1}{T} - \frac{1}{298.15}\right)\right] a_H^{n_{OH}} \end{array}\right] A_n \left|1 - \Omega_n^\theta\right|^\eta, \tag{5}$$

where superscripts or subscripts nu, H and OH indicate neutral, acid and alkaline mechanisms, respectively, and a is the activity of the corresponding species.

For carbonate minerals, dissolution/precipitation mechanisms are catalyzed by bicarbonate ions (HCO_3^-), and reaction rates depend on the activity of aqueous CO_2 (carbonates mechanism). In this case, r_n is calculated using the following equation:

Table 1 Kinetic parameters for mineral dissolution and precipitation (Palandri and Kharaka 2004)

	Acid mechanism			Neutral mechanism		Carbonate/Base mechanism		
	$\text{Log}\, k^{H}$	E_a^H	n_H	$\text{Log}\, k^{nu}$	E_a^{nu}	$\text{Log}\, k^{CO_2/OH}$	$E_a^{CO_2/OH}$	n_{CO_2}/n_{OH}
Calcite	−0.30	14.40	1.00	−5.81	23.50	−3.48	35.4	1.00
Dolomite	−3.19	36.10	0.50	−7.53	52.20	−5.11	34.80	0.50
Siderite[a]	−3.19	36.10	0.50	−7.53	52.20	−5.11	34.80	0.50
Illite-Mg	−12.71	48.00	0.22	−14.41	48.00	−14.41	48.00	−0.13
Albite	−10.16	65.00	0.457	−12.56	69.80	−15.60	71.00	−0.572
K-Feldspar	−10.06	51.70	0.500	−12.41	38.00	−21.20	94.10	−0.823
Kaolinite	−11.31	65.90	0.777	−13.18	22.20	−17.05	17.90	−0.472
Chalcedony	–	–	–	−13.99	87.70	–	–	–
Magnesite	−6.38	14.40	1.00	−9.34	23.50	−5.22	62.80	1.00
Dawsonite	–	–	–	−7.00	62.80	–	–	–
Anhydrite	–	–	–	−3.19	14.30	–	–	–
Halite	–	–	–	−0.21	7.40	–	–	–

[a] Kinetic data for siderite are assumed to be equivalent of those of dolomite (Gunter et al. 2000)

$$r_n = \left[\begin{array}{l} k_{25}^{nu} \exp\left[\frac{-E_a^{nu}}{R}\left(\frac{1}{T} - \frac{1}{298.15}\right)\right] \\ \quad + k_{25}^{H} \exp\left[\frac{-E_a^{H}}{R}\left(\frac{1}{T} - \frac{1}{298.15}\right)\right] a_H^{n_H} \\ \quad + k_{25}^{CO_2} \exp\left[\frac{-E_a^{CO_2}}{R}\left(\frac{1}{T} - \frac{1}{298.15}\right)\right] a_{CO_{2,aq}}^{n_{CO_2}} \end{array} \right] A_n \left|1 - \Omega_n^{\theta}\right|^{\eta} \quad (6)$$

The parameters in the kinetic rate equation are shown in Table 1. Acid-catalyzed, base-catalyzed and neutral kinetic mechanisms are used in this simulation.

Following the mineral dissolution and precipitation, the reservoir porosity and permeability are calculated at each time step. Porosity changes in the matrix are directly related to the volume changes resulting from mineral precipitation and dissolution. Matrix permeability changes are calculated from porosity changes using the Carman–Kozeny relationship (Bear 1972). The poor knowledge of the structural characteristics of the investigated reservoir rock prevented the use of more complex porosity/permeability relationships depending on factors, such as pore size distribution, pore shapes and connectivity. Changes in porosity and permeability also have an impact on capillary pressure which is upscaled using the Leverett scaling relation (Slider 1976). These calculations are done in the chemical part of TOUGHREACT and the feedback effect of changes in porosity, permeability and capillary pressure is considered on fluid flow calculations in the hydrodynamic part of the code.

3.2 Geometrical Model

A 2D radial model is proposed as a conceptual framework for determining the transient evolution of the geochemical reactivity induced by the injection of CO_2. The 20-m thick reservoir is centred on a vertical injection well (Fig. 2). The maximum radial extent is 100 km. The system under consideration is represented by 1,190 grid blocks comprising the model mesh. The radius of the injection cell is 0.3 m. Along the radius axis, 99 grid cells are considered between 0.3 and 1,000 m, 50 grid cells between 1,000 m and 10 km, and 20 grid cells between 10 and 100 km. In each interval, the width of the radial elements follows a

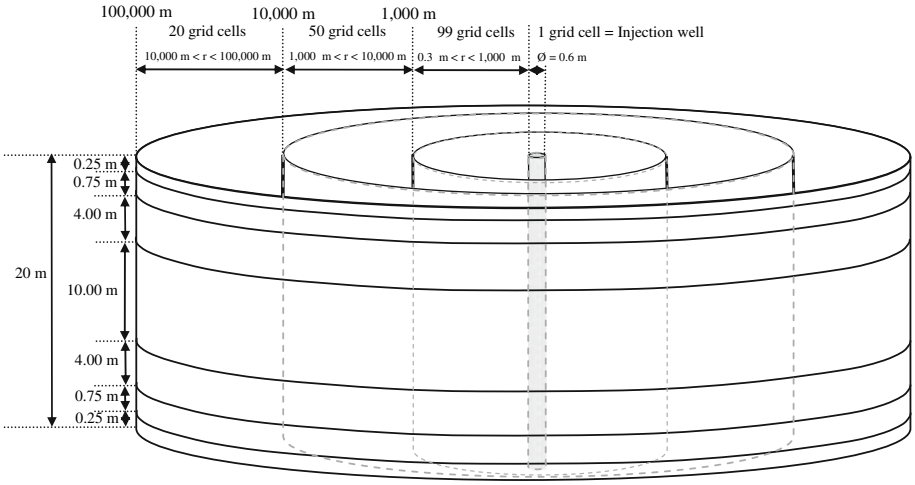

Fig. 2 Geometrical 2D radial model for supercritical CO_2 injection in a carbonate reservoir. The diameter of the injection well is 0.6 m whereas the first element adjacent to the wellbore presents a width of 0.32 m

logarithmic scale. The objective of such refinement near the injection well is to capture more precisely both the details of geochemical processes and the migration of the desiccation front in the near-well region. The vertical discretization is achieved by a division of the reservoir into seven layers. The seven reservoir layers are, from bottom to top, 0.25, 0.75, 4, 10, 4, 0.75 and 0.25 m thick.

The bedrock and caprock are assumed to be impervious, whereas thermal conduction from the bedrock and caprock to the reservoir is taken into account. In TOUGH2, the method of Vinsome and Westerveld (1980) is used to integrate heat exchanges between reservoir fluids and the confining beds. This method is based on a semi-analytical approach that prevents meshing outside of the fluid flow domain. The vertical layers close to the bedrock and caprock are thinner in agreement with the numerical constraints of vertical heat exchanges (i.e. thermal gradient, heat conductivity, time step etc.).

No regional flow is considered and a hydrostatic status is initially assumed for the pressure within the reservoir and maintained constant at the lateral boundary. The initial temperature and pressure of the targeted reservoir are 75°C and 18 MPa, respectively.

The physical properties of the reservoir are those of the Dogger aquifer in the Paris Basin. This regional reservoir, with a mean depth of 1,600–1,700 m, has a porosity of 0.15. Reservoir permeability is anisotropic, with a horizontal permeability of 10^{-13} m^2 (100 mD) and a vertical permeability of 10^{-14} m^2 (10 mD) ($K_V/K_H = 0.1$). Mainly composed of carbonates, its rock grain density approaches 2,750 kg m^{-3}. The formation heat conductivity and the rock grain specific heat are 2.51 W m^{-1} °C and 900 J kg^{-1} °C, respectively (Rojas et al. 1989).

The experimental capillary pressure and the liquid relative permeability were fitted using the Van Genuchten model, whereas gas relative permeability was fitted with a fourth-degree polynomial function (André et al. 2007). The parameters used in the simulations for liquid relative permeability and capillary pressure models are summarized in Table 2.

During the brine evaporation process driven by dry CO_2 injection, the capillary pressure is limited to a maximum value of 10 MPa. This value is quite large, but it is not unreasonable when compared to values proposed by many authors who predict values up to 100 MPa during the desiccation process of a porous medium (Rossi and Nimmo 1994; Pettenati et al. 2008 and references cited therein).

Table 2 Van Genuchten parameters used for fitting the characteristic curves for brine (i.e. relative permeability and capillary pressure), whereas a polynomial correlation was used for the relative permeability of the gas phase (see André et al. 2007 for greater detail)

Relative permeability parameters for brine	
(Van Genuchten model—1980)	
$m = 1 - 1/n$	0.600
Residual liquid saturation	0.200
Liquid saturation	1.000
Residual gas saturation	0.050
Capillary pressure parameters (Van Genuchten model—1980)	
$m = 1 - 1/n$	0.600
Residual liquid saturation	0.199
P_0 (Pa)	54,000
P_{max} (Pa)	10^7
Liquid saturation	1.0

Table 3 Dogger aquifer mineralogy and list of minerals not initially present in the reservoir but able to precipitate

Mineral composition	Volume fraction
Primary minerals	
Calcite	0.70
Dolomite	0.10
Siderite	0.05
Illite	0.05
Albite	0.05
K-Feldspar	0.05
Secondary minerals (potentially precipitating minerals)	
Kaolinite	0.00
Chalcedony	0.00
Magnesite	0.00
Dawsonite	0.00
Anhydrite	0.00
Halite	0.00

3.3 Mineralogical Assemblage

The Dogger reservoir consists mainly of carbonates (85% by volume calcite, disordered dolomite and siderite) with some alumino-silicates (albite and K-Feldspar) and illite (Rojas et al. 1989). Minerals that can precipitate as secondary phases during CO_2 injection are kaolinite, chalcedony, magnesite, dawsonite, anhydrite and halite (Table 3).

3.4 Water Chemistry

While the Dogger reservoir contains water with salinity values ranging from moderate ($3\,g\,kg^{-1}$ of water) to high ($35\,g\,kg^{-1}$ of water in the deepest part of the aquifer), in this study, only a moderately saline brine ($5\,g\,kg^{-1}$ of water) is assumed (Table 4) (Michard and

Table 4 Chemical composition of Dogger aquifer water in the low salinity part of the reservoir (concentrations in ppm)

Temperature	75°C
pH	6.70
Alkalinity	427.0
Na	1,794.0
K	35.2
Ca	148.0
Mg	55.9
Al	0.002
Fe	1.0
Cl	2,485.0
SO_4	633.6
SiO_2	41.4
HS	11.9

Bastide 1988). This water is initially at thermodynamic equilibrium with all the minerals initially present in the reservoir. The partial pressure of carbon dioxide (pCO_2) governs the equilibrium of the solution with calcite and the pH of the water results from this equilibrium with carbonate rocks (calcite and disordered dolomite; Michard and Bastide 1988). Silicon concentration is correlated with reservoir temperature and is in agreement with chalcedony solubility (Azaroual et al. 1997).

4 Numerical Simulations

The results of two injection scenarios are presented here. The numerical simulations were done by coupling thermal, hydraulic and chemical processes (THC simulations). The first scenario uses a low injection flow rate ($1\,kg\,s^{-1}$) and the second, a high injection flow rate ($20\,kg\,s^{-1}$). For Scenario 1, two injection temperatures are used: 75 and 40°C. The higher temperature (i.e. the reservoir temperature) is used to highlight the role of internal thermal effects (role of petrophysical properties and thermodynamic constraints). The lower temperature was selected to have a maximum difference relative to the reservoir temperature (with an anthropic origin) but also to maintain CO_2 in the supercritical state.

The specified downhole temperatures are constant for the two scenarios during the entire injection period, and the injected CO_2 is dry (absolutely no water). The CO_2 is injected into the thickest layer of the reservoir, i.e. the 10-m layer at mid-depth to increase the pressure gradient close to the injection well and thus, amplify thermal processes as the Joule–Thomson effect.

In this study, the injection period is quite short (about 300 days), because only the near-well region is explored. The reactivity close to the injection well is emphasized because it will have a direct impact on well injectivity and the integrity of the well completion.

4.1 Scenario 1: Coupled Simulations (THC) at Low Flow Rate ($1\,kg\,s^{-1}$)

Supercritical CO_2 is injected at a very low flow rate ($1\,kg\,s^{-1}$) enabling us to define and quantify the major physical, thermal and geochemical processes occurring in the near-well region and within the reservoir at different spatial and time scales. The injection temperatures

are 75°C (Scenario 1A) and 40°C (Scenario 1B). The objective of Scenario 1A is to verify the conclusions in André et al. (2007) and to determine whether the geometrical model (2D radial vs. 1D radial) has an impact on the results. Scenario 1B is used to determine the role of temperature on chemical reactivity.

4.1.1 Within the Entire Impacted Area (Large Scale)

The injection of CO_2 causes a small increase in pressure. The maximum build-up occurs near the well (with an increase of about 0.5 MPa) but the pressure impact has spread 5,000 m around the injection well after 300 days. A second key point concerns the extension of the gas bubble and the position of the two-phase front within the reservoir. As CO_2 solubility in water at this pressure and temperature is about 1 mol kg_w^{-1}, all the injected CO_2 cannot be dissolved in the formation water and a two-phase system (supercritical CO_2—saline water) develops within the reservoir. The injected CO_2 pushes the formation water away from the injection well by a piston-like effect. After 300 days, the gas bubble extends about 200 m around the injection well at the top of the reservoir and 50 m at the bottom (Fig. 3a). The spreading is not uniform within the reservoir due to relative permeability and viscosity effects (phase mobility) against gravity forces. This simulation also shows that with such an injection period and low flow rate (1 kg s^{-1}), no desiccation occurs close to the injection well.

The chemical composition of the groundwater in the reservoir is impacted by the injected CO_2. Carbon dioxide dissolution increases the acidity of the medium, enabling mineral dissolution (mainly of carbonates). The groundwater pH is buffered to about 4.8 due to the equilibrium between the water and carbonate minerals. As the radius of the CO_2 bubble increases, the flowing brine composition in the area between the two-phase displacement front and the dry-out front is governed by gas–fluid–rock exchanges. This thermodynamic equilibrium state between these phases does not permit to dissolve more and more carbonates during the brine flow preventing any massive spatially localized dissolution of native reservoir minerals. However, due to the shape of the gas front, mineralogical reactivity is greater at the top of the reservoir (Fig. 3b). Calcite is the most reactive mineral, with dissolved quantities five times greater near the interface with the caprock than at mid-depth in the reservoir. Dolomite does not present the same behaviour, with a more regular dissolution in the upper part of the reservoir. Some weak dissolutions of siderite, albite and K-Feldspar are also observed in the upper part of the reservoir. The spatial variations of chemical reactivity depend only on CO_2 concentration and pH (no thermal effect, Fig. 4). As CO_2 moves upward into the aquifer, the acidity increases at the top of the reservoir and mineral dissolution occurs, in particular, near the interface with the caprock. Near the interface with the basement, the reactivity is negligible because the CO_2 does not reach this region.

Far from the injection well (100–250 m), the temperature effects are insignificant and only the heat-of-dissolution of CO_2 is observable (Fig. 4). However, this temperature increase alone cannot explain the differences in chemical reactivity.

4.1.2 Within 10 m of the Injector (Near-Well Region)

Thermal effects are greater near the injection well (0–50 m, Fig. 4). Many thermal processes are involved, e.g. the Joule–Thomson cooling effect and the enthalpy of water evaporation close to the well. Due to the weak pressure gradient at this injection rate, the Joule–Thomson cooling effect is, however, small, with variations of about 1°C.

For Scenario 1A, the temperature gradients are very low (Fig. 4a). The consequence is a weak influence of temperature on mineralogical reactivity. This is confirmed at 10 m from the

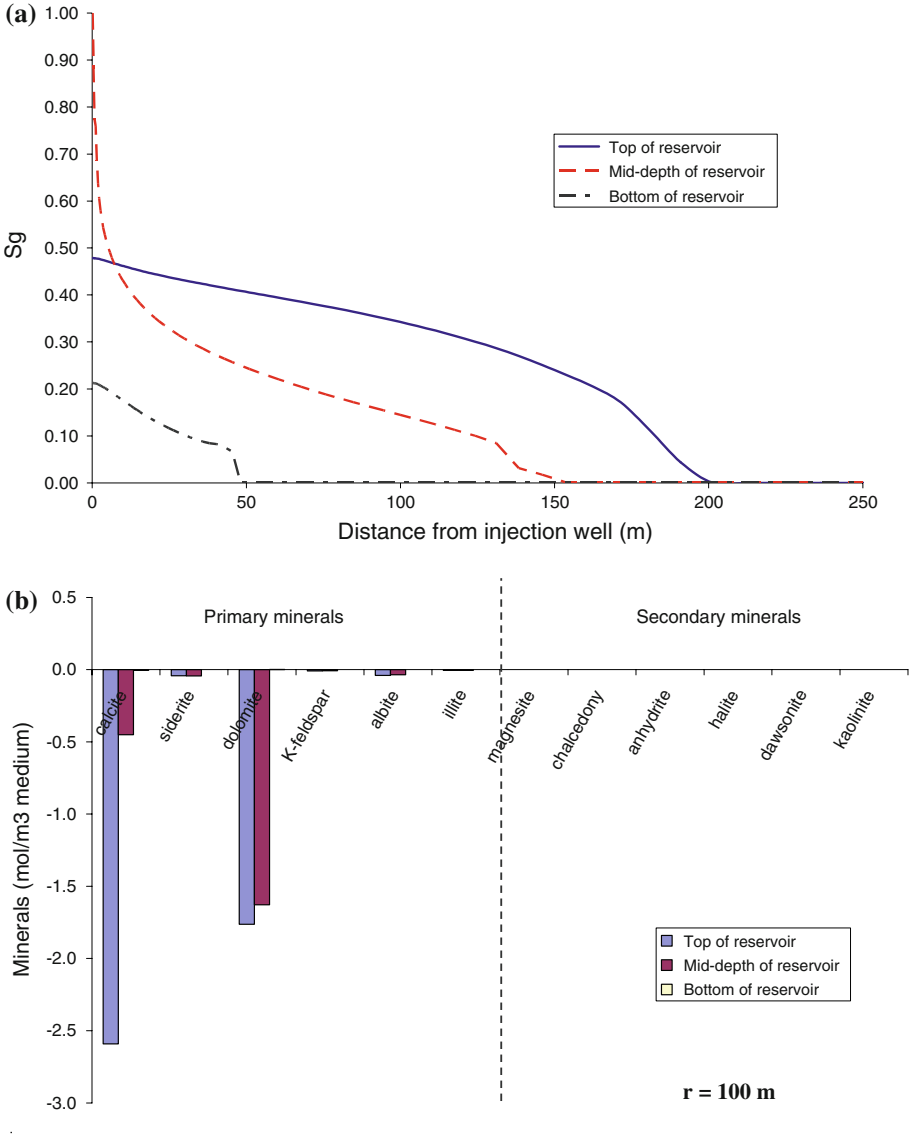

Fig. 3 Results obtained with Scenario 1A: **a** Spatial evolution of gas saturation within the reservoir after a 300-day period of supercritical CO_2 injection at 1 kg s^{-1} and 75°C; **b** Quantity of dissolved minerals (mostly carbonates) 100 m from the injection well

injector, a zone where the CO_2 concentration is quite constant on a vertical profile (Fig. 3a). The dissolution of carbonates (dolomite, calcite and siderite) and other primary minerals (albite, K-Feldspar) is homogeneous (Fig. 5a).

Closer to the injector, the behaviour of different minerals is highly variable (Fig. 5b). As dry CO_2 is injected at mid-depth in the reservoir, water evaporation occurs preferentially. Residual water, trapped in micropores, evaporates and minerals can precipitate. Dolomite and siderite precipitate, whereas calcite continues to dissolve (Fig. 5b). Because the CO_2

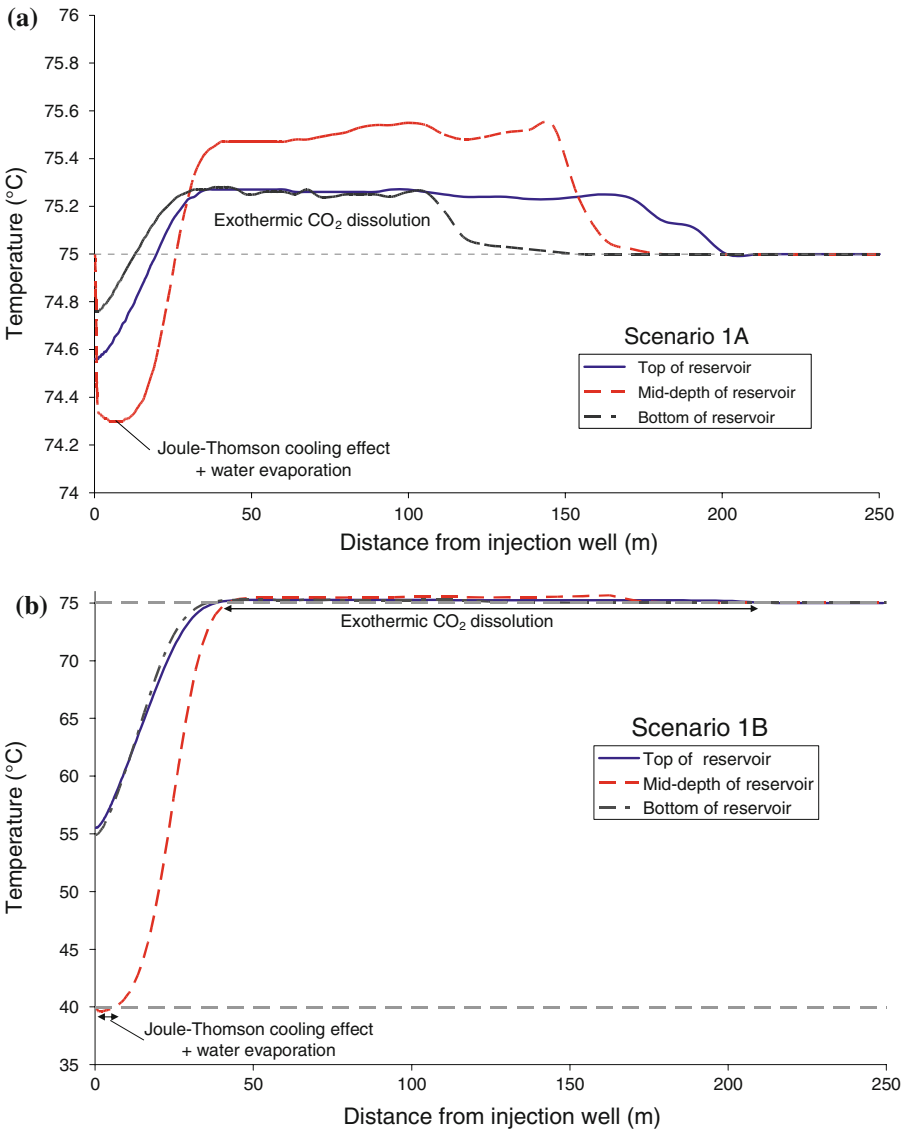

Fig. 4 Spatial evolution of temperature within the reservoir after a 300-day period of supercritical CO_2 injection at $1\,kg\,s^{-1}$: **a** at 75°C; **b** at 40°C. *Note*: The vertical scale is different in **a** and **b**. *Grey dashed lines* represent the initial reservoir temperature (75°C) and the CO_2 injection temperature (40°C)

injection flow rate is low, the desiccation process does not appear to be advanced enough to enable the precipitation of salts. Only primary minerals are affected by this process.

For Scenario 1B, Fig. 4b clearly shows that major temperature gradients are observed in the first 10 m from the injection well, mainly due to the injection temperature ($T_{inj} = 40°C$). The temperature is not uniform within the reservoir, and differences of about 20°C are expected between reservoir mid-depth and reservoir edges. Consequently, highly variable mineralogical reactivity is expected in this zone (Fig. 6). Ten meters from the injector, dolomite

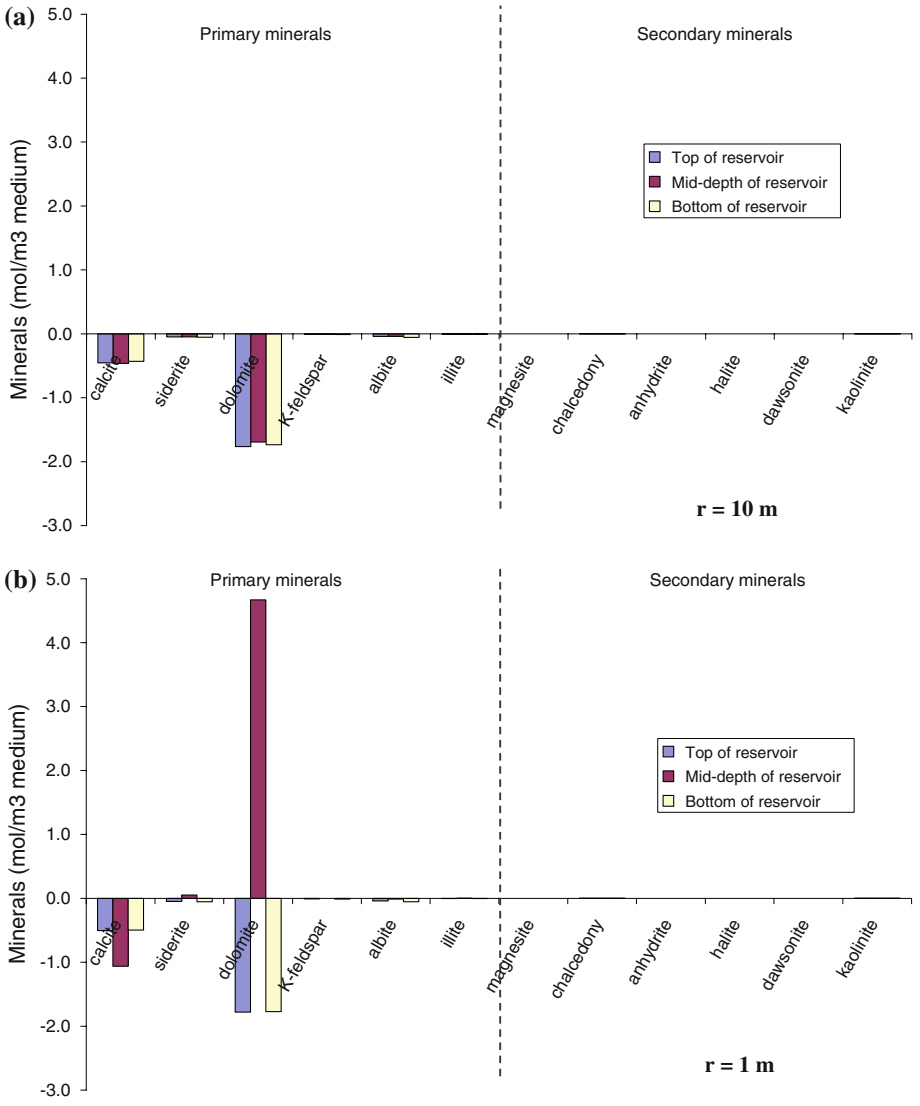

Fig. 5 Results obtained with Scenario 1A—variations in mineral concentrations around the injection well after a 300-day period of supercritical CO_2 injection (flow rate = 1 kg s^{-1} and $T = 75°C$): **a** 10 m; **b** 1 m. Negative values correspond to dissolution and positive values to precipitation

dissolution is about 50% greater at reservoir mid-depth than at the reservoir edges (Fig. 6a). The difference in chemical reactivity is essentially caused by temperature effects: low temperatures increase both CO_2 dissolution and carbonate solubility (Plummer and Busenberg 1982). One meter from the injection well, there is more calcite dissolution at reservoir mid-depth than close to the interfaces with the caprock and basement, whereas there is 25% less dissolution of dolomite and siderite at reservoir mid-depth than on the edges (Fig. 6b). An explanation for this can be seen in Fig. 7. First, there is more dolomite and siderite dissolution in Scenario 1B than in Scenario 1A due to a low injection temperature. Second, due to

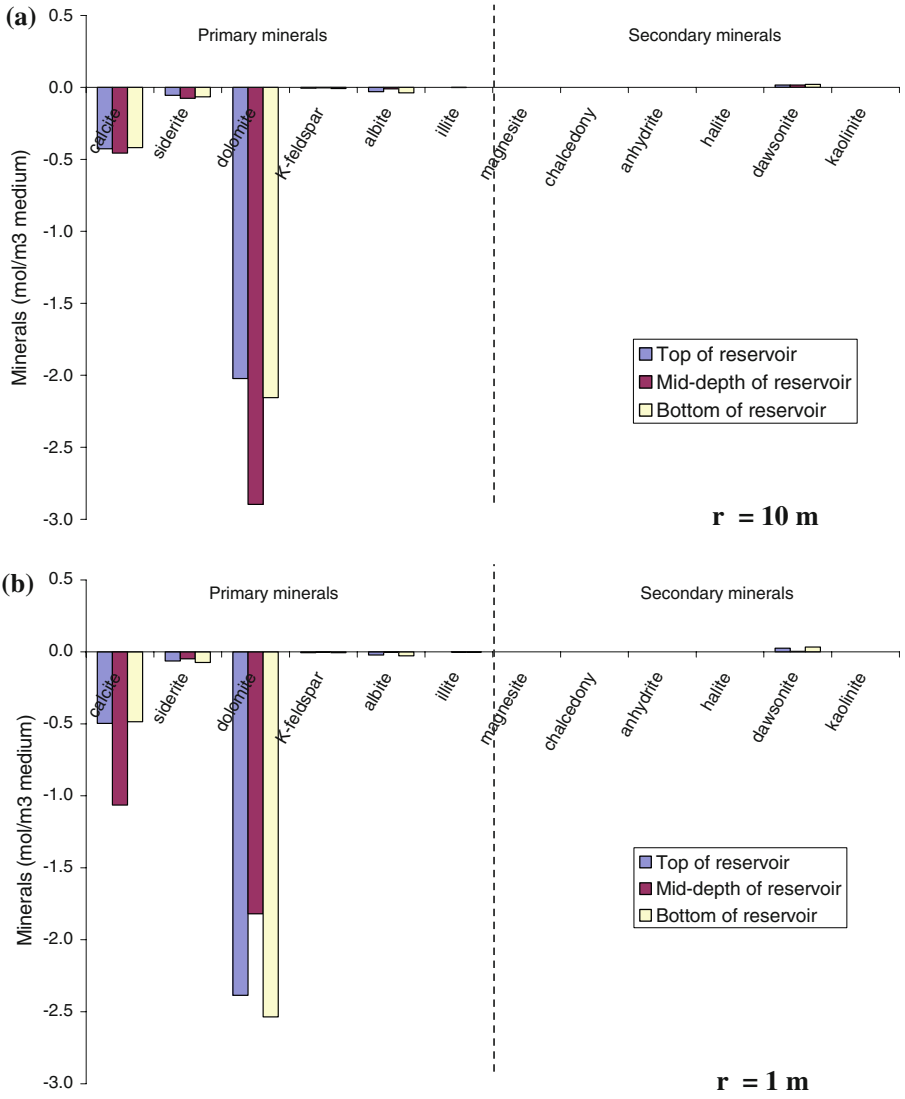

Fig. 6 Results obtained from Scenario 1B—variation in mineral concentrations around the injection well after a 300-day period of supercritical CO_2 injection (flow rate = 1 kg s^{-1} and $T = 40$°C): **a** 10 m; **b** 1 m. Negative values correspond to dissolution and positive values to precipitation

desiccation, the dolomite and siderite precipitation period follows the dissolution period at mid-depth in the reservoir.

The start of this phase and its magnitude differ in Scenarios 1A and 1B: dolomite and siderite precipitation begins 100 days later and with a lower magnitude in Scenario 1B. The geochemical process seems to be influenced by temperature with larger dolomite and siderite deposits at 75°C (Fig. 5b) than at 40°C (Fig. 6b). Precipitation of dawsonite also seems to be temperature-dependent. No deposits are observed at 75°C whereas some precipitation is

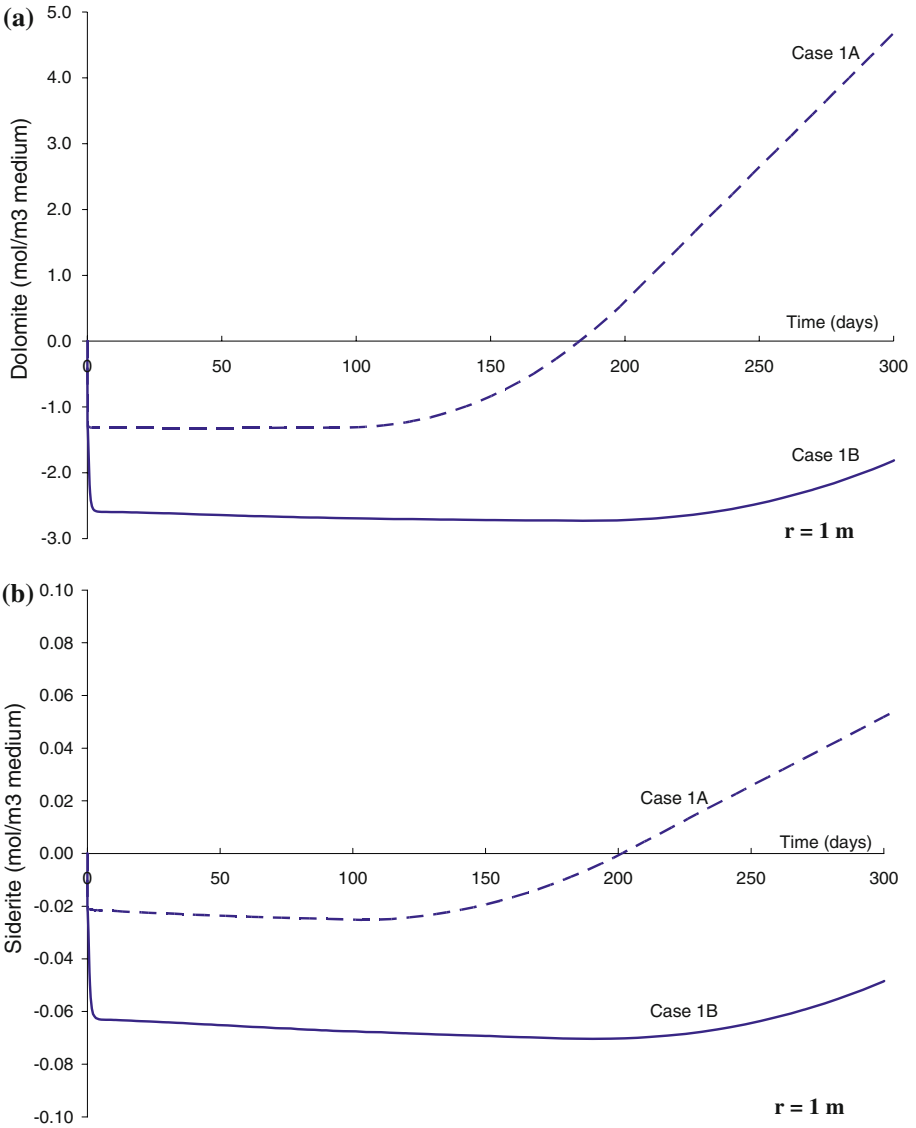

Fig. 7 Variation in dolomite (**a**) and siderite (**b**) concentrations 1 m from the injection well at mid-depth in the reservoir for Scenarios 1A and 1B

observed at 40°C. Traces of dawsonite are observed mainly on the edges of the reservoir, 1 and 10 m from the injection well (Fig. 6).

The impact of temperature on dolomite reactivity can be clearly seen when the dolomite concentration around the injection well is plotted for Scenarios 1A and 1B (Fig. 8). Dolomite dissolution is greater in Scenario 1B in the reservoir zone where the temperature is lower than 60°C (Fig. 4b). A dissolution ratio of 2 is observed between the low-temperature zone (0–30 m) and the high-temperature zone (beyond 30 m).

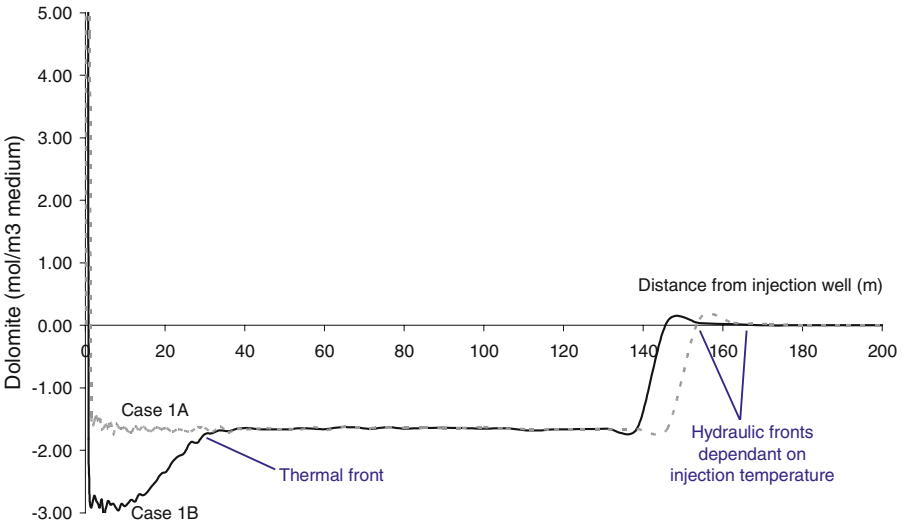

Fig. 8 Relative variations of dolomite concentration after a 300-day period of supercritical CO_2 injection in the reservoir mid-depth for the Scenarios 1A and 1B

The results using Scenario 1A are in good agreement with previous results obtained on a 1D radial model (André et al. 2007). 1D and 2D calculations confirm that, in a first step, the injection of CO_2 into a carbonate reservoir causes the dissolution of carbonates (calcite, dolomite and siderite). Other primary minerals such as albite and K-Feldspar also dissolve due to acidification, but to a lesser extent. Furthermore, the 1D and 2D approaches both show that the near-well region (less than 5 m from injector) is affected by mineral precipitation. Dolomite seems to be the most reactive mineral and it precipitates first. The 1D simulation was done with a long-term injection period (10 years) and salt precipitation (anhydrite) was observed. The simulation period in Scenario 1A (300 days) is too short to observe this type of phenomenon. Nevertheless, this 2D approach goes further than the 1D approach, and enables us to predict the spatial reactivity of the system. While the 1D calculation gave simply the radius of mineral precipitation, the 2D model provides information concerning the vertical position of the deposits and the architectural structure of active geochemical reactions.

4.2 Scenario 2: Coupled Simulation (THC) at High Flow Rate (20 kg s^{-1}) and Injection Temperature of 40°C

This numerical simulation uses a scenario in which supercritical CO_2 is injected at an industrial flow rate (20 kg s^{-1}) and a temperature of 40°C, lower than the initial reservoir temperature. The aim is to determine the impact of reservoir cooling, induced by a massive injection of CO_2, on chemical reactivity.

4.2.1 Within the Entire Impacted Area (Large Scale)

Whereas reservoir pressure was not significantly affected by CO_2 injection in Scenario 1, supercritical CO_2 injection at a higher flow rate (×20) causes a large increase in pressure throughout the reservoir. In the first 20 km around the injection well, the pressure grows, with a maximum increase from 18 MPa to up to 23.5 MPa close to the injection well (Fig. 9a). As

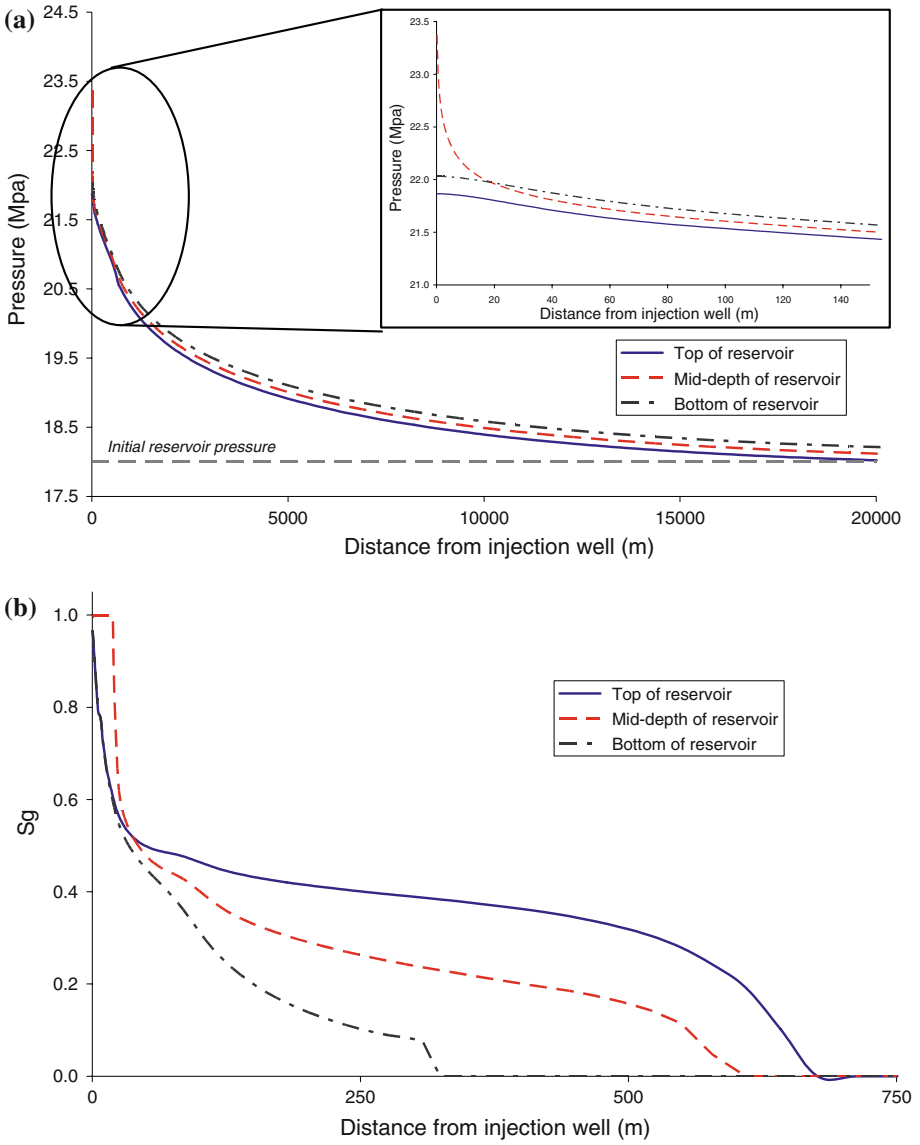

Fig. 9 Results obtained with Scenario 2 after a 300-day period of supercritical CO_2 injection at 20 kg s^{-1} and 40°C: **a** Spatial evolution of pressure within the reservoir (with enlargement of 0–150 m); **b** Spatial evolution of gas saturation within the reservoir

injected gas moves into the mid-depth of the reservoir, the maximum build-up of pressure is significant in the centre of the aquifer. Pressure near the interfaces is quite similar with higher values at the bottom of the reservoir due to gravity. Beyond 40 m, the pressure gradient between the top and the bottom of the reservoir does not exceed 0.2 MPa (Fig. 9a).

Similar to what occurs in Scenario 1, the massive CO_2 injection leads to the formation of a two-phase system (supercritical CO_2 and brine). Depending on temperature and pressure conditions, part of the injected CO_2 dissolves in the groundwater whereas the remaining

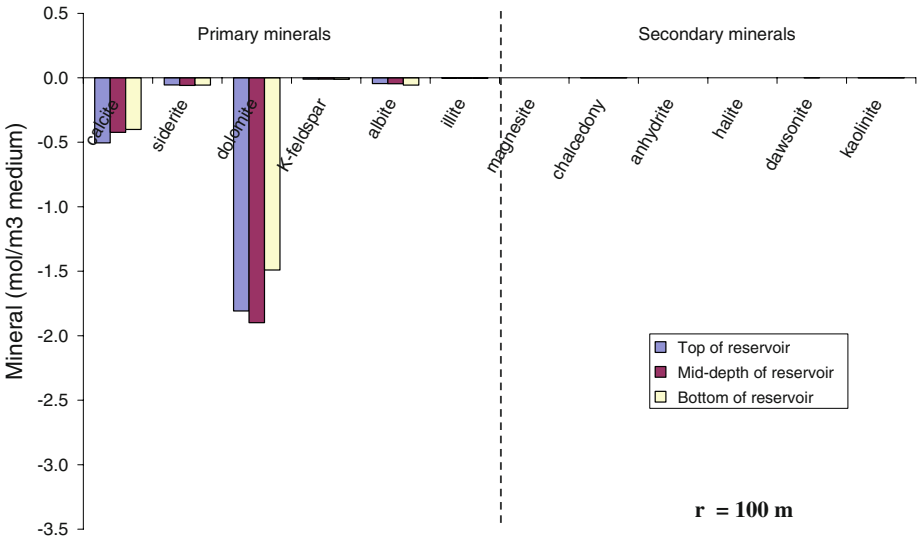

Fig. 10 Results obtained with Scenario 2—variation in mineral concentrations 100 m from the injection well after a 300-day period of supercritical CO_2 injection (flow rate = 20 kg s^{-1} and $T = 40°C$)

CO_2 stays in its own supercritical state. Figure 9b shows the evolution of gas (supercritical) saturation within the reservoir. After 300 days of injection, desiccation occurs in the grid cells located at mid-depth in the reservoir within a radius of about 20 m. Although the injection flow rate is high, the CO_2 distribution in the reservoir is driven by an upward movement of supercritical CO_2 close to the top interface (Fig. 9b).

Far from the injection well (100–300 m), the chemical reactivity at a given vertical profile is constant. Figure 10 shows that carbonates, in particular, are affected by CO_2 injection. While calcite and dolomite are the most dissolved minerals, siderite, albite and K-Feldspar are also impacted by acidification of the medium. The similarity of Figs. 10 and 5a is very interesting. It shows that the injection flow rate does not have an impact on elementary and fundamental chemical processes (carbonate and mineral dissolution) but only on the location within the reservoir where these processes occur. With the increase in the injection flow rate, the chemical processes occur farther from the injector.

4.2.2 Within 100 m of the Injector (Near-Well Region)

The injection of cold supercritical CO_2 (40°C) causes a decrease in temperature in the near-well region. Different processes can be identified (Fig. 11):

- In the first 20 m, where desiccation is total, the Joule–Thomson effect is expressed. It is about 1°C, correlated with the pressure gradient presented in Fig. 9a.
- Between 20 and 50 m, a greater decrease of temperature is observed (enlargement in Fig. 11). Some of this temperature gradient is due to the Joule–Thomson effect (in the same order of magnitude as what was observed between 0 and 20 m), whereas another part is due to water evaporation. In this zone, the temperature gradient between the mid-depth and the edges of the reservoir is greatest and reaches 10–15°C depending on the location in the reservoir and the period of CO_2 injection.

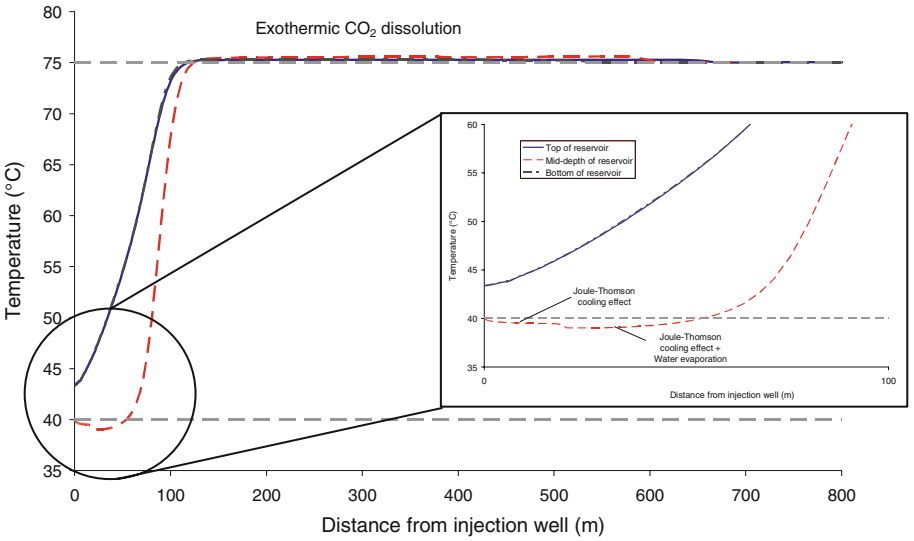

Fig. 11 Results obtained with Scenario 2: spatial evolution of temperature within the reservoir after a 300-day period of supercritical CO_2 injection at 20 kg s^{-1} and 40°C with enlargement of the first 100 m. *Grey dashed lines* at 75 and 40°C represent the initial reservoir temperature and the CO_2 injection temperature, respectively

– Between 50 and 100 m, the temperature increases gradually. The thermal front moves into the reservoir as a function of the imposed flow rate.
– Between 100 and 700 m, the dissolution of CO_2 generates a weak temperature increase (about 0.5–1°C).

Injection at high flow rate and low temperature has many consequences on the chemical reactivity of the system. First, as in Scenario 1B and outside of the desiccation zone, carbonates (dolomite, calcite and siderite) dissolve whereas dawsonite precipitates as traces (Fig. 12a). The chemical pattern observed at a distance of 10 m in Scenario 1B (Fig. 6a) is observed 30 m from the injection well in Scenario 2. The reservoir mid-depth is also the most reactive zone with an increase in dolomite dissolution of about 40% with respect to the edges. This increase in dolomite reactivity is related to the solubility of carbonates with respect to temperature (Plummer and Busenberg 1982).

Closest to the injection well, in the desiccation zone (1–10 m), opposite processes are highlighted: dolomite and siderite precipitate in the mid-depth reservoir zone whereas calcite dissolves (Fig. 12b, c).

Due to the complete desiccation of the porous medium, secondary minerals precipitate as anhydrite, halite and dawsonite. The largest deposits (halite, in particular) are observed at mid-depth in the reservoir where desiccation is total. One meter from the injection well, traces of anhydrite appear on the edges of the reservoir. The desiccation in these grid cells is underway and only traces of salts are observable. As gas saturation is not maximum on the edges of the reservoir, the dissolution of carbonates and other minerals continues even after a 300-day period of injection (Fig. 12b, c).

Albite, illite and K-Feldspar dissolve slightly far from the injection well (Fig. 12a), whereas these minerals seem to be deactivated closer to the injection well (Fig. 12b, c). The spatial changes in geochemical processes are related to the injection flow rate and the dissolution/precipitation kinetics of the minerals involved. Close to the injection well, the high injection flow

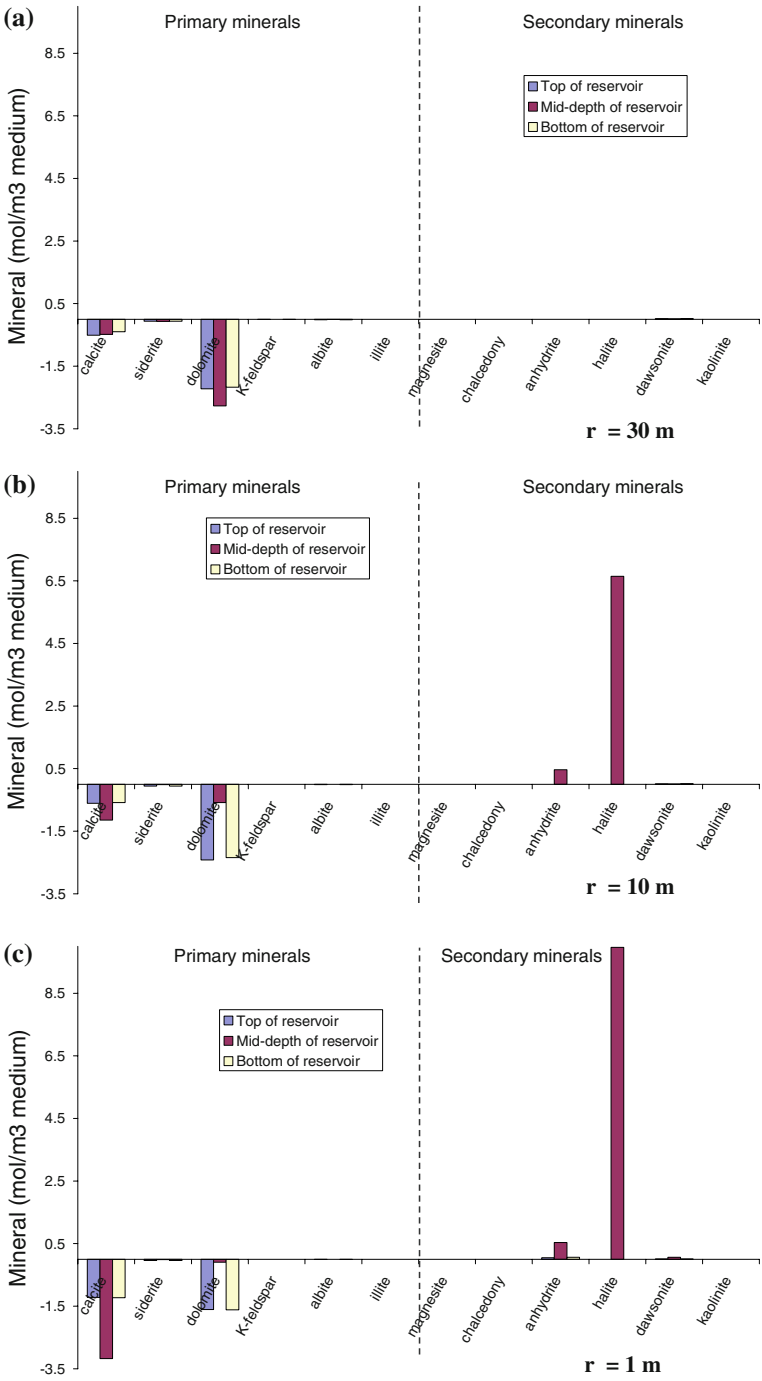

Fig. 12 Results obtained with Scenario 2: variations in mineral concentrations around the injection well after a 300-day period of supercritical CO_2 injection (flow rate = 20 kg s^{-1} and $T = 40°C$): **a** 30 m; **b** 10 m; **c** 1 m. Negative values represent dissolution whereas positive values represent precipitation

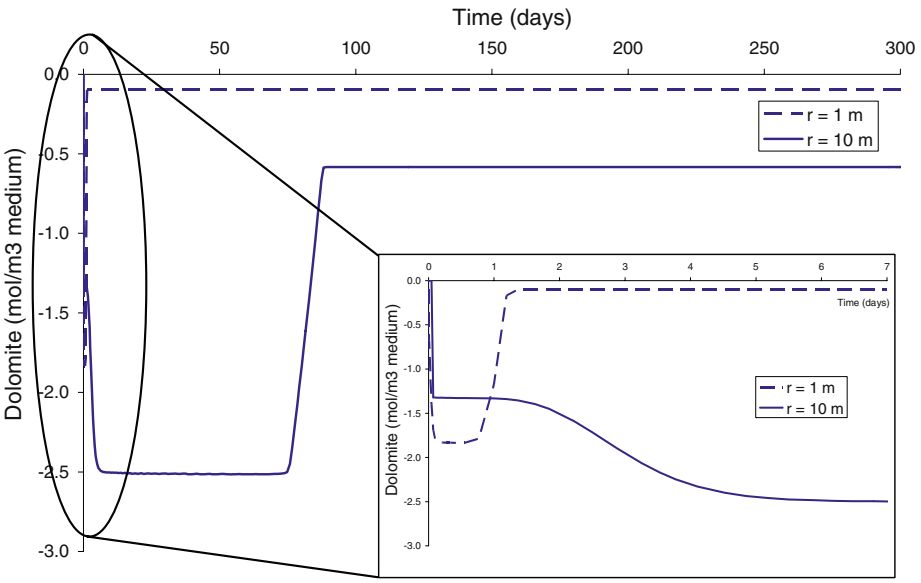

Fig. 13 Variation in dolomite concentrations during CO_2 injection 1 and 10 m from the injection well at mid-depth in the reservoir. After 300 days, the targeted zone is fully desiccated

rate generates relatively high fluid velocities. As the kinetics of the alumino-silicate minerals are slow, the residence time of acidified brine is too short for the minerals to dissolve or precipitate. Far from the well, fluid velocity decreases and minerals have enough time to react (long residence time).

Scenario 2 shows that the chemical processes involved in this scenario are roughly the same as those in Scenario 1B (flow rate = 1 kg s^{-1}; $T = 40$°C). Dissolution and precipitation of minerals are highlighted in both scenarios although the location and magnitude of these processes can be different (Fig. 13). The increase in the CO_2 injection flow rate displaces the processes farther in the reservoir. In Scenario 1B, at a distance of 1 m from the injection well, dolomite precipitation began after 200 days of injection (Fig. 7a). In Scenario 2, the process is very rapid, and in less than 2 days, dolomite dissolves then precipitates and chemical reactivity stops because all water has been removed from the porous medium. This reaction wave is also recorded 10 m from the injection well. The carbonated mineral first dissolves (with a larger magnitude than at 1 m) and then precipitates until the medium has dried out completely (after about 70 days).

Figure 13 also confirms that mineral reactivity is influenced by the injection flow rate. As shown for alumino-silicate minerals (Fig. 12b, c), the lower reactivity of dolomite at 1 m when compared to at 10 m (Fig. 13) shows that even minerals with high kinetic rate constants are influenced by higher flow rates. Injection controls the overall system, as opposed to gravity and the chemical reactivity of the system. Fluid transfers increase and chemical reactivity is affected by these high flow rates. The chemical reaction zones and their extents are directly linked to the fluid transfer dynamics as generally characterized by the dimensionless Damköhler number (Knapp 1989).

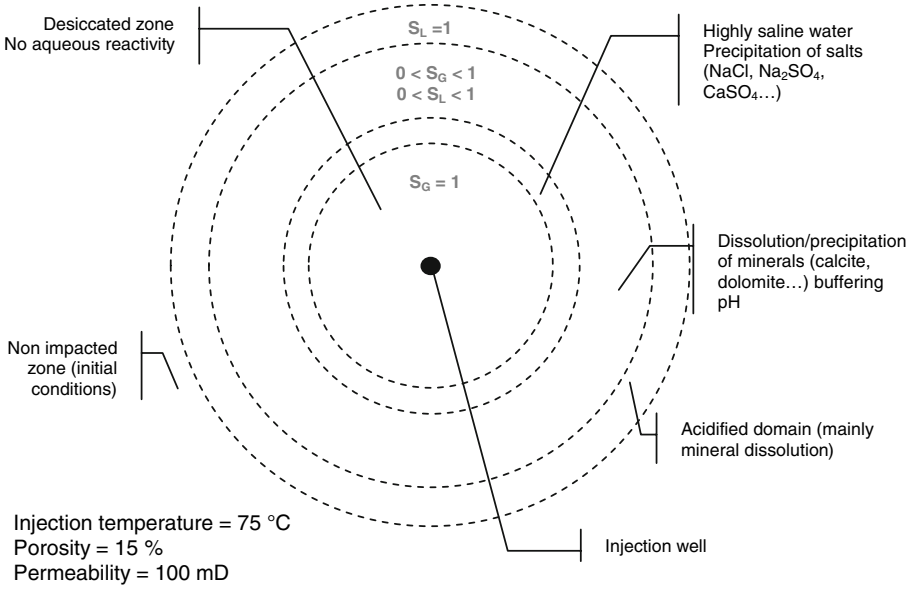

Fig. 14 Typical radii of processes occurring in the near-well region after CO_2 injection in a saline aquifer (Azaroual et al. 2007; Gaus et al. 2008)

5 Discussion

This study, which is an extension of André et al. (2007) and Pruess (2009), examined the geochemical reactivity of a carbonate reservoir by means of different simulations. Different scenarios with various injection flow rates and injection temperatures are investigated.

At low flow rate and high temperature (Scenario 1A), the results obtained with a 2D radial model are in agreement with the results of André et al. (2007). Injecting CO_2 into a carbonate reservoir dissolves carbonates (calcite, dolomite and siderite) in the area near the injector. Albite and K-Feldspar are also weakly dissolved due to acidification of native and residual groundwater. However, following this dissolution phase, there is mineral precipitation due to evaporation due to the injection of dry CO_2: dolomite seems to be the most reactive mineral and precipitates first. The reactivity tendency and the geochemical mechanisms presented in Fig. 14 are confirmed by these simulations.

The 2D approach goes further and enables us to predict the spatial reactivity of the system within the reservoir. At low flow rate and low injection temperature (Scenario 1B), we observe the same geochemical reactivity as that observed for Scenario 1A far from the injection well. This shows that the thermal effects are spatially limited. Close to the injection well, the temperature gradients have an impact on the chemical reactivity of the system, mainly on dolomite precipitation, which decreases at low temperature. This is encouraging because it shows that injection at low temperature (<60°C) decreases carbonate reactivity, sustaining the injectivity. This behaviour is caused by the retrograde solubility of carbonates (increased solubility at low temperature). Moreover, siderite presents the same behaviour as dolomite, whereas calcite does not follow the same reactive pathway. These varying behaviours of carbonate minerals must initiate some highly diffusive and mixing processes due to the nearer positions of Ca and CO_3 sources (calcite) and sinks (dolomite and siderite).

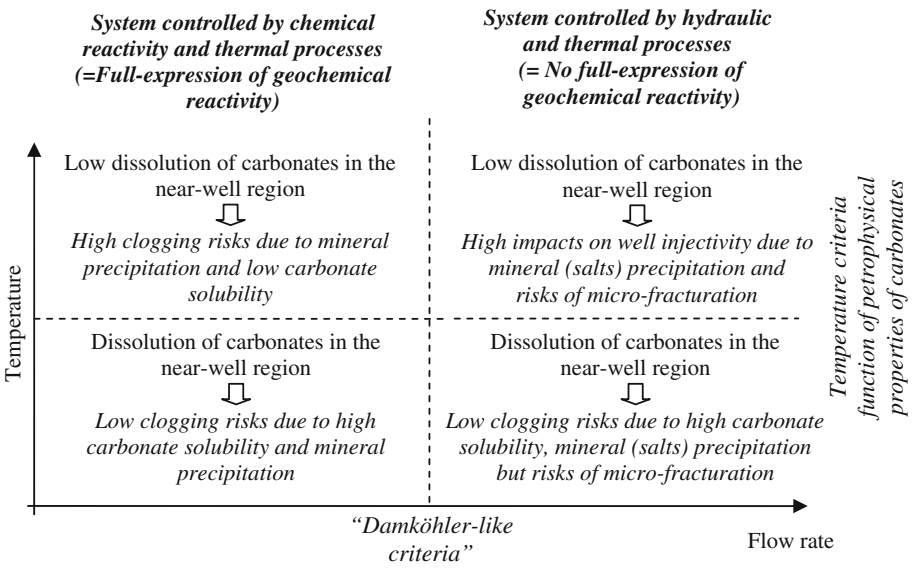

Fig. 15 Injection scenarios as a function of injection temperature and supercritical CO_2 flow rate in carbonate reservoirs. The dimensionless 'Damköhler-like criteria' determine the boundary between the fictive conditions where the rate of chemical reactions is higher than the advection rate (*on the left*) and those where the hydraulic processes are dominant (*on the right*). The two temperature-dependent domains at elevated flow rates refer to carbonates reactivity and their dissolution potentials

At high flow rate and low temperature (Scenario 2), the chemical processes that occur are the same as those observed in Scenario 1B. The change of the flow rate influences only the location within the reservoir where the chemical processes occur. The increase in the CO_2 injection flow rate shifts the reactive processes farther from the injection well. Injection at high flow rate also causes the drying-out of the porous medium and the precipitation of salts such as halite. No clogging of the porous medium is observed but this is mainly due to the initial composition of the groundwater (low salinity, around $5\,g\,kg_w^{-1}$). The highly diluted solution prevents any massive salts deposits.

These simulations highlight the influence of hydraulic forces, gravity forces, temperature effects and the chemical reactivity of the system (Fig. 15). All of these phenomena are expressed due to the careful selection of flow rates and injection temperatures. The examples developed in Scenario 1 show that a low injection flow rate leads to the total expression of chemical processes: all the minerals have enough time to react with the liquid solution.

The fate of the system is controlled by chemical reactivity (under kinetic and thermal constraints) which in turn counteracts hydraulic processes. Although the short-term injection period does not show this, an extreme consequence of such chemical reactivity near the injector could lead to the clogging of the porous medium (depending on the salinity of the initial groundwater and the volumetric balance between dissolved and precipitated minerals). Nevertheless, due to the retrograde solubility of carbonates, the risk of clogging seems limited at low temperature (with less carbonate precipitation) and might support the recommendation to inject at reduced temperature.

Scenario 2 describes a fictive 'industrial' CO_2 injection with influencing hydraulic processes (due to high injection flow rates) and low residence times of reactive fluids in the near-well region. The simulation performed at low temperature (remarkably lower than the

reservoir temperature) demonstrates that CO_2 injection fosters carbonate dissolution (particularly in the reservoir mid-depth). Thereafter, due to the high injection flow rate, the desiccation of the porous medium is very rapid and involves the precipitation of primary and secondary minerals, but massive deposition is avoided. This behaviour, which indicates a limited reactivity of minerals due to kinetic effects, activation energy in particular (Table 1), is very interesting for carbonate reservoirs, and particularly in low-permeability carbonate aquifers. A low CO_2 injection temperature seems to constitute an interesting approach for increasing carbonate dissolution and well injectivity. The drawback of CO_2 injection at low temperature and high flow rate is the possible micro-fissuring of the porous medium due to the temperature gradient and salt precipitation (similar to the very well-known local overpressure caused by salt deposition—La Iglesia et al. 1997; Steiger and Asmussen 2008). The mechanical aspects of the rock are not only taken into consideration in this study but also they will have to be considered for the safety and the integrity of geological storage and especially for well completion.

6 Conclusion

This study investigates the impact of the geochemical reactivity of deep carbonate aquifers subjected to supercritical CO_2 injections. THC simulations show that physical, chemical and thermal processes triggered by CO_2 injection are highly coupled and mainly affect the near-well region. The thermal processes that might occur in deep carbonate aquifers have been investigated and different processes have been identified. Close to the injection well, the Joule–Thomson effect was identified, mainly in the desiccated zone. However, its effect on reservoir temperature is relatively minor due to the low Joule–Thomson coefficient at the temperature and pressure conditions of the reservoir studied. Since pressures are higher than 150 bar, the Joule–Thomson coefficient is low and the magnitude of temperature changes less than 1–2°C. The heat of water evaporation and heat-of-dissolution of CO_2 in the groundwater have also been estimated. Latent heat can be observed in a restricted zone during the evaporation process. It is combined with the Joule–Thomson effect and maximum variations of about 2–3°C are expected. The heat-of-dissolution can be observed over a large scale. Injected CO_2 is very mobile in the reservoir and CO_2 dissolution affects large areas even if CO_2 solubility is limited ($<1.5\,\mathrm{mol\,kg_w^{-1}}$). Consequently, heat-of-dissolution is a diffuse thermal process that affects large zones but the magnitude of the effect is small (increase of about 1°C). The thermal process with the greatest influence is the temperature of the injected CO_2. It is difficult to predict the downhole temperature because it is dependent on injection conditions at the surface. However, the injection temperature will probably be different from the reservoir temperature (and probably lower in the case of very deep saline reservoirs). Simulations at low injection temperature show that we can expect to find large temperature gradients between the centre of thick aquifers and the interfaces with caprock and basement.

Our conclusion about thermal processes, if they are taken individually, is that they have little to no effect on the overall behaviour of the reservoir. However, in an integrated approach, these thermal processes are of interest as they govern both the fluid state (liquid, gaseous or supercritical CO_2) and the chemical reactivity of the system. The impact of thermal processes will have to be considered mainly in three types of scenarios:

– for deep reservoirs presenting temperature and pressure conditions close to those of the critical point of CO_2, like at the Ketzin site (Bielinski et al. 2008);

– for deep reservoirs presenting temperature and pressure conditions favourable to a good expression of the Joule–Thomson coefficient, like in depleted gas fields (Oldenburg 2007);
– if the injection temperature is very different from the reservoir temperature (Scenario 2 of the present study). The scenarios proposed here highlight the sensitivity of a carbonate system to injection temperature.

Acknowledgements This study was carried out within the framework of the 'GeoCarbone-Proche Puits' project, co-funded by the French National Agency for Research (ANR). The authors are grateful for Curt Oldenburg for making its recommendations, and for two anonymous reviewers for helpful comments and suggestions.

References

André, L., Audigane, P., Azaroual, M., Menjoz, A.: Numerical modeling of fluid-rock chemical interactions at the supercritical CO_2-liquid interface during supercritical carbon dioxide injection into a carbonated reservoir, the Dogger aquifer (Paris Basin, France). Energy Convers. Manag. **48**, 1782–1797 (2007)

Azaroual, M., Fouillac, C., Matray, J.M.: Solubility of silica polymorphs in electrolyte solutions, II. Activity of aqueous silica and solid silica polymorphs in deep solutions from the sedimentary Paris Basin. Chem. Geol. **140**(3–4), 167–179 (1997)

Azaroual, M., Kervévan, C., Durance, M.V., Brochot, S., Durst, P.: SCALE2000 (V3.1): Logiciel de calculs thermodynamiques et cinétiques applicables aux saumures pétrolières, hydrothermales et industrielles (*User's Manual in French*). BRGM, ISBN 2-7159-0939-X (2004)

Azaroual, M., Pruess, K., Fouillac, C.: Feasibility of using supercritical CO_2 as heat transmission fluid in the EGS (Enhanced Geothermal Systems) integrating the carbon storage constraints. In: ENGINE—Enhanced Geothermal Innovative Network for Europe. Workshop 2: Exploring High Temperature Reservoirs: New Challenges for Geothermal Energy, SIAF Campus, Volterra, Italy, 1–4 April 2007

Bachu, S.: Sequestration of CO_2 in geological media in response to climate change: road map for site selection using the transform of the geological space into CO_2 phase space. Energy Convers. Manag. **43**, 87–102 (2002)

Bear, J.: Dynamics of Fluids in Porous Media. American Elsevier, New York (1972)

Bielinski, A., Kopp, A., Schütt, H., Class, H.: Monitoring of CO_2 plumes during storage in geological formations using temperature signals: numerical investigation. Int. J. Greenh. Gas Control **2**, 319–328 (2008)

Brown, D.: A hot dry rock geothermal energy concept utilizing supercritical CO_2 instead of water. In: Proceedings of the Twenty-Fifth Workshop on Geothermal Reservoir Engineering, Stanford University, 2000, pp. 233–238

Gaus, I., Audigane, P., André, L., Lions, J., Jacquemet, N., Durst, P., Czernichowski-Lauriol, I., Azaroual, M.: Geochemical and solute transport modelling for CO_2 storage, what to expect from it? Int. J. Greenh. Gas Control **2**, 605–625 (2008)

Gunter, W.D., Perkins, E.H., Hutcheon, I.: Aquifer disposal of acid gases: modelling of water–rock reactions for trapping of acid wastes. Appl. Geochem. **15**(8), 1085–1095 (2000)

Helgeson, H.C., Kirkham, D.H., Flowers, G.C.: Theoretical prediction of the thermodynamic behaviour of aqueous electrolytes at high pressures and temperatures. 4. Calculation of activity coefficients, osmotic coefficients, and apparent molal and standard and relative partial molal properties to 600°C and 5 kb. Am. J. Sci. **281**, 1249–1516 (1981)

Intergovernmental Panel on Climate Change: Chapter 5: Underground geological storage. In: Metz, B., et al. (eds.) Special Report on Carbon Dioxide Capture and Storage. Cambridge University Press, Cambridge (2005)

Knapp, R.B.: Spatial and temporal scales of local equilibrium in dynamic fluid-rock systems. Geochim. Cosmochim. Acta **53**(8), 1955–1964 (1989)

Koschel, D., Coxam, J.-Y., Rodier, L., Majer, V.: Enthalpy and solubility of CO_2 in water and NaCl(aq) at conditions of interest for geological sequestration. Fluid Phase Equilib. **247**, 107–120 (2006)

La Iglesia, A., González, V., López-Acevedo, V., Viedma, C.: Salt crystallization in porous construction materials: I. Estimation of crystallization pressure. J. Cryst. Growth **177**, 111–118 (1997)

Lasaga, A.C.: Chemical kinetics of water-rock interactions. J. Geophys. Res. **89**(B6), 4009–4025 (1984)

Lassin, A., Azaroual, M., Mercury, L.: Geochemistry of unsaturated soil systems: aqueous speciation and solubility of minerals and gases in capillary solutions. Geochim. Cosmochim. Acta **69**(22), 5187–5201 (2005)

Lu, M., Connell, L.D.: Non-isothermal flow of carbon dioxide in injection wells during geological storage. Int. J. Greenh. Gas Control **2**, 248–258 (2008)
Mahadevan, J.: Flow-through drying of porous media. PhD Dissertation, The University of Texas at Austin (2005)
Mahadevan, J., Sharma, M.M., Yortsos, Y.C.: Water removal from porous media by gas injection: experiments and simulation. Transp. Porous Med. **66**, 287–309 (2007)
Marcolini, M., Geloni, C., Battistelli, A., Gherardi, F., Biagi, S.: Near wellbore processes and water-rock reactions driven by the geologic sequestration of dry CO_2 in a natural gas layer. Geophysical Research Abstract, 10, EGU2008-A-09323, 5th EGU General Assembly (2008)
Michard, G., Bastide, J.-P.: Etude géochimique de la nappe du Dogger du Bassin de Paris. J. Volcanol. Geotherm. Res. **35**, 151–163 (1988)
Oldenburg, C.M.: Joule–Thomson cooling due to CO_2 injection into natural gas reservoirs. Energy Convers. Manag. **48**, 1808–1815 (2007)
Palandri, J., Kharaka, Y.K.: A compilation of rate parameters of water-mineral interaction kinetics for application to geochemical modelling. US Geological Survey Open File Report 2004-1068, p. 64 (2004)
Pan, L., Oldenburg, C.M., Wu, Y.S., Pruess, K.: Wellbore flow model for carbon dioxide and brine. Energy Procedia **1**, 71–78 (2008)
Paterson, L., Lu, M., Connell, L.D., Ennis-King, J.: Numerical modelling of pressure and temperature profiles including phase transitions in carbon dioxide wells. In: SPE 115946, Presented at the 2008 SPE Annual Technical Conference and Exhibition in Denver, Colorado, USA, 21–24 September 2008
Pettenati, M., Mercury, L., Azaroual, M.: Capillary geochemistry in non-saturated zone of soils. Water content and geochemical signatures. Appl. Geochem. **23**, 3799–3818 (2008)
Plummer, L.N., Busenberg, E.: The solubilities of calcite, aragonite and vaterite in CO_2-H_2O solutions between 0 and 90°C, and an evaluation of the aqueous model for the system $CaCO_3$-CO_2-H_2O. Geochim. Cosmochim. Acta **46**(6), 1011–1040 (1982)
Pruess, K.: Behaviour of CO_2 injection wells. In: 3rd Annual Conference on Carbone Capture and Sequestration, Alexandria, VA, 3–6 May 2004
Pruess, K.: ECO2n: a TOUGH2 fluid property module for mixtures of water, NaCl and CO_2. Lawrence Berkeley National Laboratory Report LBNL-57952, Berkeley, CA, USA (2005)
Pruess, K.: On production behavior of enhanced geothermal systems with CO_2 as working fluid. Energy Convers. Manag. **49**, 1446–1454 (2008)
Pruess, K., Oldenburg, C.M., Moridis, G.J.: TOUGH2 user's guide, version 2.0. Lawrence Berkeley National Laboratory Report LBNL-43134, Berkeley, CA, USA (1999)
Pruess, K., Azaroual, M.: On the feasibility of using supercritical CO_2 as heat transmission fluid in an engineered hot dry rock geothermal reservoir. In: Proceedings of the Thirty-First Workshop on Geothermal Reservoir Engineering, Stanford University, Stanford, CA, USA, 2006, pp. 386-393
Pruess, K.: Modelling of non-isothermal effects in CO_2 storage. In: CO_2 Geological Storage Modelling Workshop, Orléans, France, 10–12 February 2009
Rojas, J., Giot, D., Le Nindre, Y.M., Criaud, A., Fouillac, C., Brach, M., et al.: Caractérisation et modélisation du réservoir géothermique du Dogger, bassin parisien, France. Rapport final CCE, EN 3G-0046-F(CD), BRGM R 30 IRG SGN 89 (1989)
Rossi, C., Nimmo, J.R.: Modeling of soil water retention from saturation to oven dryness. Water Resour. Res. **30**, 701–708 (1994)
Slider, H.C.: Practical Petroleum Reservoir Engineering Methods, p. 559. Petroleum Publishing Company, Tulsa (1976)
Spycher, N., Pruess, K.: CO_2-H_2O mixtures in the geological sequestration of CO_2. II: Partitioning in chloride brines at 12-100°C and up to 600 bars. Geochim. Cosmochim. Acta **69**(13), 3309–3320 (2005)
Steefel, C.I., Lasaga, A.C.: A coupled model for transport of multiple chemical species and kinetic precipitation/dissolution reactions with applications to reactive flow in single phase hydrothermal system. Am. J. Sci. **294**, 529–592 (1994)
Steiger, M., Asmussen, S.: Crystallization of sodium sulfate phases in porous materials: the phase diagram Na_2SO_4-H_2O and the generation of stress. Geochim. Cosmochim. Acta **72**, 4291–4306 (2008)
Van Genuchten, M.T.: A closed-form equation for predicting the hydraulic conductivity of unsaturated soils. Soil Sci. Soc. Am. J. **44**, 892–898 (1980)
Vidal-Gilbert, S., Nauroy, J.-F., Brosse, E.: 3D geomechanical modelling for CO_2 geologic storage in the Dogger carbonates of the Paris Basin. Int. J. Greenh. Gas Control **3**(3), 288–299 (2009)
Vinsome, P.K.W., Westerveld, J.: A simple method for predicting cap and base rock heat losses in thermal reservoir simulators. J. Can. Pet. Technol **19**(3), 87–90 (1980)
Weir, G.J., White, S.P., Kissling, W.M.: Reservoir storage and containment of greenhouse gases. Transp. Porous Med. **23**(1), 37–60 (1996a)

Weir, G.J., White, S.P., Kissling, W.M.: Reservoir storage and containment of greenhouse gases: II. Vapour-entry pressures. Transp. Porous Med. **23**(1), 61–82 (1996b)

White, S.P., Allis, R.G., Moore, J., Chidsey, T., Morgan, C., Gwynn, W., Adams, M.: Simulation of reactive transport of injected CO_2 on the Colorado Plateau, Utah, USA. Chem. Geol. **217**, 387–405 (2005)

Wolery, T.: EQ3/6: software package for geochemical modelling of aqueous systems: package overview and installation guide (version 7.0). Lawrence Livermore National Laboratory Report UCRLMA-110662 PTI. Livermore, California (1992)

Xu, T., Pruess, K.: Modeling multiphase non-isothermal fluid flow and reactive geochemical transport in variably saturated fractured rocks: 1. Methodology. Am. J. Sci. **301**, 16–33 (2001)